




Abstract

The chemical properties of stars are normally derived from spectroscopic measurements, where such properties can give astronomers a glimpse into the environment in which these stars were born. However, this method can be difficult and more time consuming to obtain for low-mass stars in particular, due their relative faintness on the sky. On the other hand, photometry of low-mass stars is widely available due to the many all-sky surveys that have been conducted over the past couple of decades. To take advantage of this, we have calibrated a new relationship that predicts chemical properties of low-mass stars from multiple photometric measurements using machine learning with a Gaussian Process Regressor. We show that this regressor is able to predict these chemical properties with a high level of accuracy (± 0.11 dex), while also mitigating systematic errors that were present in previous metallicity calibration attempts. Specifically, our technique avoids these systematic errors by removing unresolved binary star systems present in our sample before training the regressor, using an iterative method described here. The addition of this step in our method is crucial, as individual properties for the stars in unresolved systems cannot be derived accurately because of the blending of light from both objects. This newly calibrated relationship now allows for the chemical properties of $\sim 10^7$ stars in the vicinity of the Sun to be estimated. These metallicities can be utilized in many areas of research. For example, we discuss here how we plan to use this relationship to study local streams in the vicinity of the Sun, and determine how their kinematic properties are related to stellar chemistry. Relationships between chemistry and kinematics of these groups will allow us to have a better understanding of the origins and histories of these streams, and relate them to dynamical interactions with spiral arms and/or bar-like features in our Galaxy.

Calibration Data


To estimate the chemical properties of a star, we use photometric measurements as inputs for our relationship. For the calibration dataset used to train our Gaussian process regressor, we use photometry from various astronomical surveys, shown to the right. All possible color combinations are used for the initial inputs, where a “color” is defined as the difference between two photometric measurements. Additionally, we obtain distance measurements for all stars in our calibration sample, so we can calculate their absolute magnitudes, i.e. the measure of the luminosity of the stars, which are also used in the initial inputs. Cross-identification of stars between these surveys is from our Bayesian cross-match of 5,827,988 high proper motion stars in Gaia (Medan, Lépine & Hartman in prep.).



Pan-STARRS
PS1 Science Consortium

Pan-STARRS¹: five optical photometric measurements (g,r,i,z,y)


Image credit: Pan-STARRS



2MASS
2 MICRON ALL-SKY SURVEY

2MASS²: three near-infrared photometric measurements (J,H,K_s)


Image credit: IPAC/CalTech



WISE

AllWISE³: two infrared photometric measurements (W1,W2)

Image credit: NASA JPL



gaia

Gaia⁴: parallax measurements, used to calculate distance

Image credit: ESA



APOGEE⁵: metallicity derived from high resolution spectra in near-infrared

Image credit: SDSS-III



Hejazi et al.⁶: metallicity derived from observations at MDM, Lick, Kitt-Peak and Cerro-Tololo Observatories

Image credit: H. Stockebrand

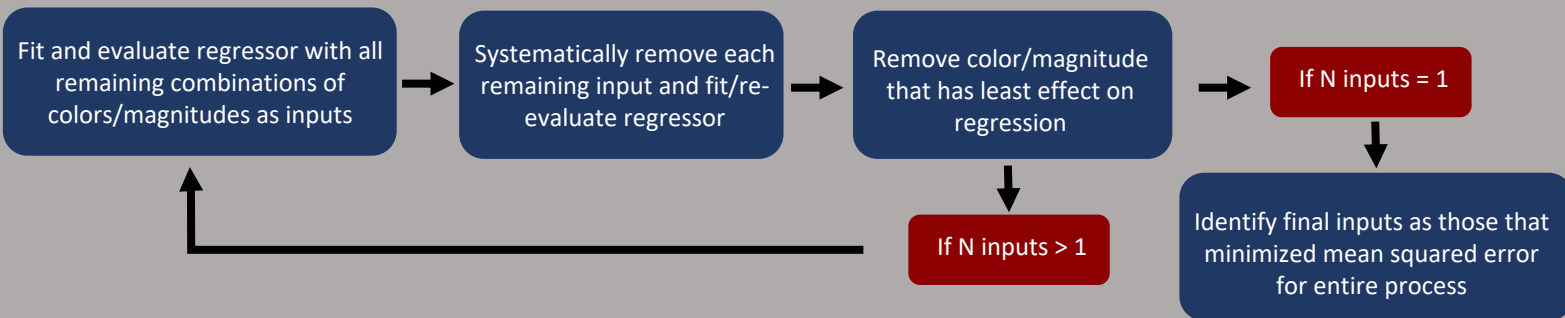
To evaluate the Gaussian Process Regressor during training, the chemical properties of the stars in the calibration sample are obtained from two spectroscopic surveys (left). For the outputs, we use the average metallicity of the stars, which is the abundance of elements heavier than hydrogen or helium. The metallicity values are determined from model fits of spectra from stars with $3500 < T_{\text{eff}} < 5280$ K, which are typical for low-mass stars. Our calibration sample comprises 6,370 stars with required inputs (photometry) and outputs (metallicity).

Photometric Metallicity Calibration Procedure

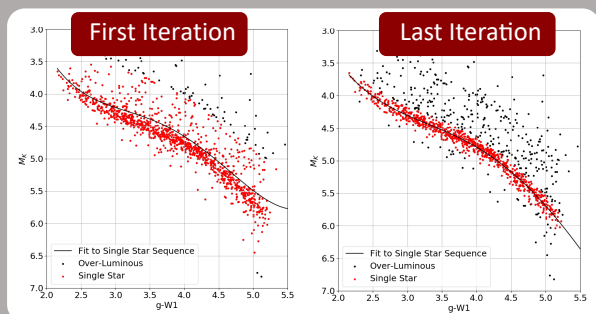
Our photometric metallicity relationship is calibrated using a Gaussian Process Regressor implemented in *scikit-learn*⁷ with an RBF kernel and a white-noise kernel proportional to the average error of the derived metallicities. Qualitatively, the RBF kernel in our Gaussian Process assumes that functional values are more correlated when the inputs are closer, as opposed to farther away. The white-noise kernel then simply adds identically distributed noise over the entire function range. Before calibration, all photometry is corrected for extinction using a 3D dust map⁸ in combination with the proper extinction law for the measurement^{9,10}. To calibrate this Gaussian Process Regressor, the following procedure is used:

STEP 1

For *Step 1*, we determine the input colors and absolute magnitudes using the iterative method shown to the right. The final color and absolute magnitude remaining during this process will be used to form the HR diagrams below in *Step 2*.

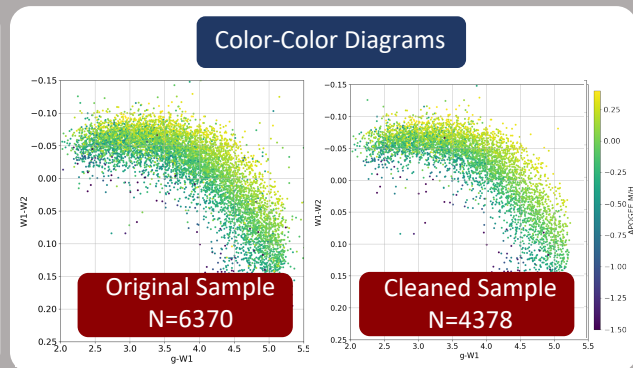
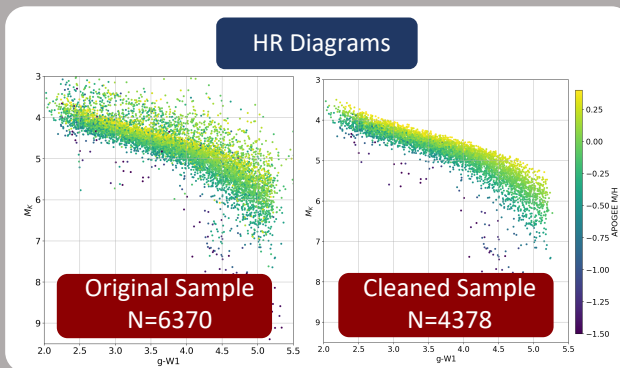


STEP 2



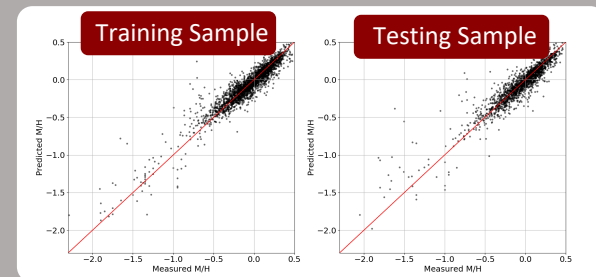
For *Step 2*, we remove unresolved binaries (UBs) from our calibration sample. 4th degree polynomials are fit to HR diagrams of absolute magnitude vs. color (from *Step 1*) in bins of average metallicity, $[M/H]=0.1$ dex. Stars that are over-/under-luminous compared to the fit, as expected of UBs, are removed (black dots). The fit is repeated and UBs removed until the solution converges and no more UBs are identified.

When comparing the HR diagram for the original sample to the cleaned sample, the sample now appears significantly cleaned after the removal of the UBs. When comparing the samples using only colors, represented with the color-color diagrams, it is clear such contaminants would not have been noticed. We find the removal of these contaminants is crucial, as metallicity values derived from spectra of UBs are unreliable due to the blending of light from both stars in the system.



STEP 3

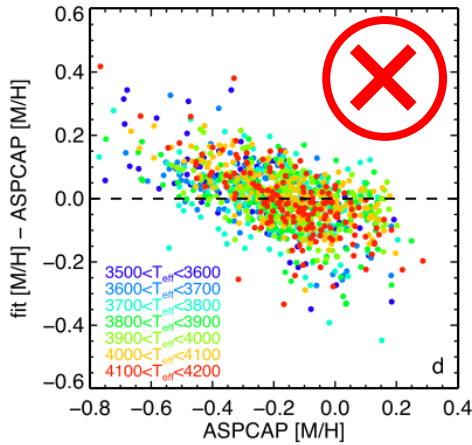
For *Step 3*, we redo the regression with the cleaned sample from *Step 2*. This includes repeating the procedure from *Step 1* to determine the input colors and magnitudes for the final Gaussian Process Regressor, but this time using the cleaned sample. This results in the following optimal inputs: M_g , $g-y$, $y-W2$, $J-W2$ and $W1-W2$. The comparison of the measured and predicted metallicity values are shown to the right for the training sample (sample used to train the regressor) and testing sample (sample used to evaluate the regressor). An average 1σ scatter of 0.11 dex is found in the testing subset.



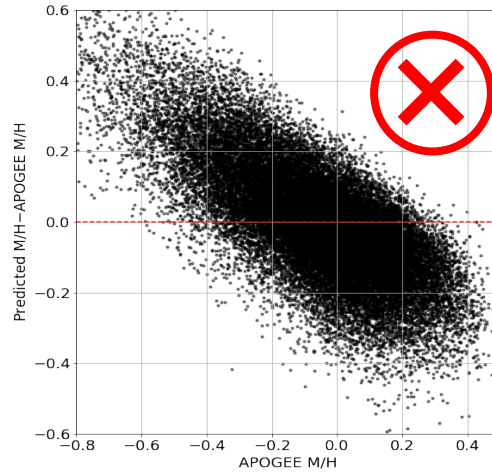
Comparing Improved Calibration

Below, we compare the results of our calibrated photometric metallicity relationship to previous studies that have used photometry in combination with metallicities from APOGEE to calibrate similar relationships. Each of these plots show the residual metallicity (i.e. difference between the predicted and measured metallicity) vs. the measured metallicity. Some of these results exhibit systematic errors where metal-poor stars' (i.e. $[M/H]<0$) metallicities are over-estimated and metal-rich stars' (i.e. $[M/H]>0$) metallicities are under-estimated. The cause of these systematics, along with summaries of each relationship, are discussed below.

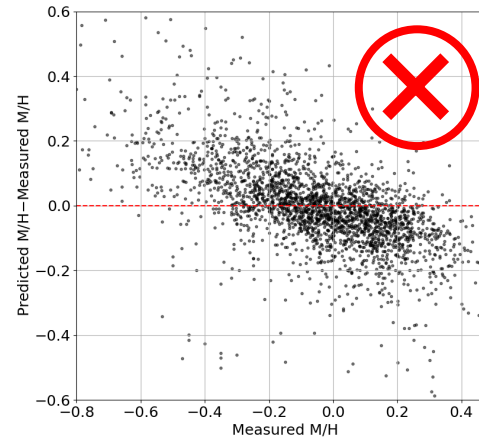
Schmidt et al.



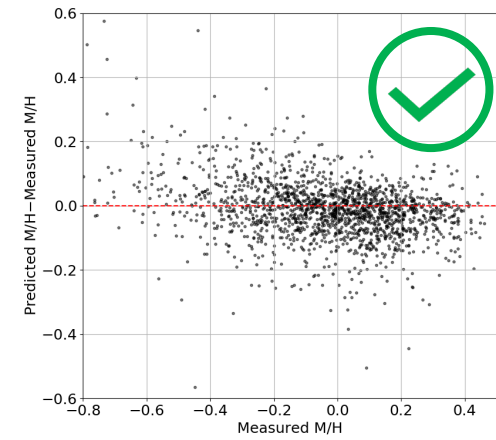
Davenport et al.



This Study – Original Sample



This Study – Cleaned Sample



Schmidt et al.¹¹ calibrated a photometric metallicity relationship using a polynomial regression to SDSS and WISE colors for a calibration sample of ~ 3800 APOGEE sources. This resulted in a relationship with a precision of ~ 0.18 dex, though systematic errors are present.

Davenport et al.¹² calibrated a photometric metallicity relationship using a k-nearest neighbors regressor to Gaia, 2MASS and WISE colors for a calibration sample of $\sim 35,000$ APOGEE sources. This resulted in a relationship with a precision of ~ 0.11 dex, though significant systematic errors are also present.

Results from the present study when the Gaussian Process Regressor is trained on the original sample that contains unresolved binaries. Systematic errors similar to past studies are observed, suggesting that such errors in these studies were due to unresolved binaries included in the calibration samples.

Results from the present study when the Gaussian Process Regressor is trained on the cleaned sample free of unresolved binaries. This results in a relationship with a precision of ~ 0.11 dex. Compared with previous calibrations, our result is largely free of systematic errors in the range of $-0.6 < [M/H] < 0.5$ dex.

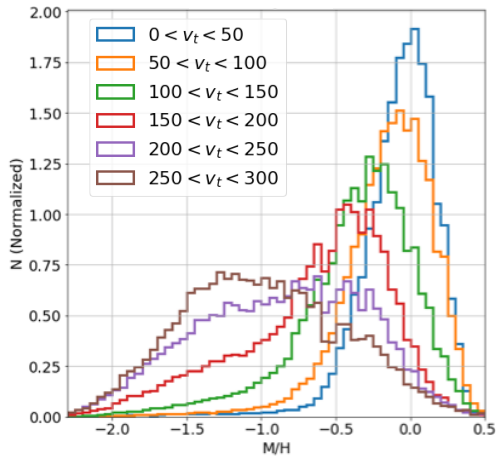
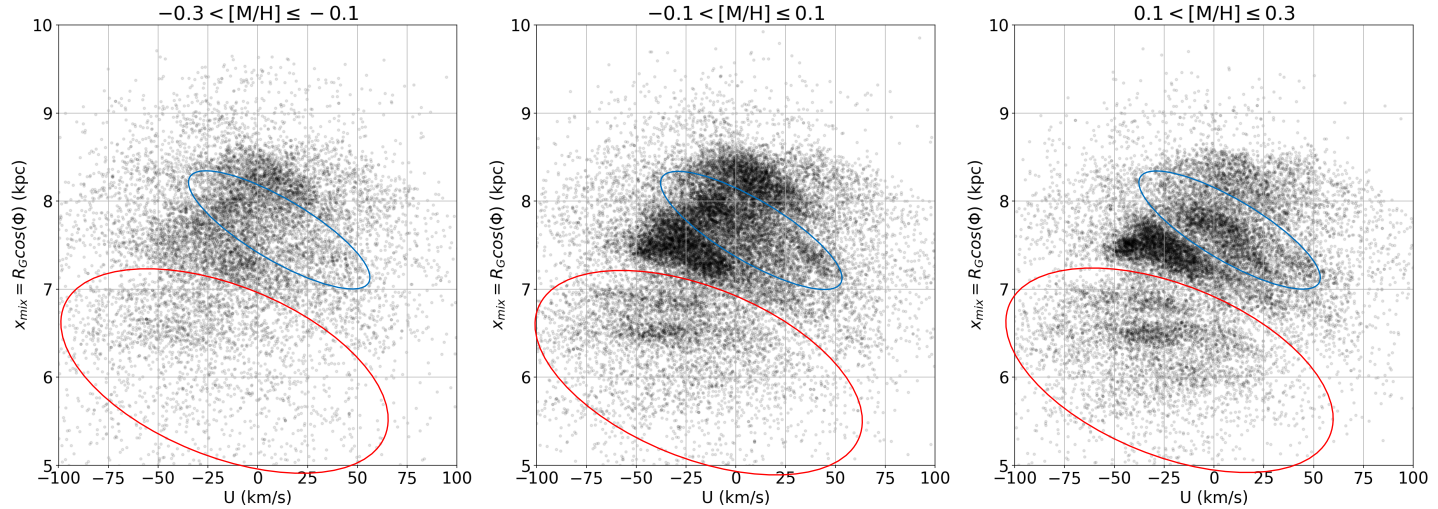
Implication of Extending Calibration

The table to right shows the number of stars in the Gaia catalog that are within 500 pc of the Sun for different temperature ranges. The top row is for the range covered by our relationship, where there are $\sim 10^7$ stars whose metallicity could be estimated. Our goal is now to calibrate a similar relationship for the cooler stars, which would double our sample. We feel that future work in extending our calibration would then be extremely beneficial to the astronomical community who benefit from this metallicity data.

Effective Temperature	Total within 500 pc	Parallax Error < 10%
$3500 < T_{\text{eff}} < 5280$ K	37,363,898	6,407,041
$T_{\text{eff}} < 3500$ K	12,430,300	5,065,645

Chemodynamical Structure

Below we examine how the metallicity of local stars relates to their kinematics by looking at the distribution in estimated metallicity from our relationship for stars with different tangential velocities. We see a general decrease in metallicity for stars with increased velocity, a trend seen in multiple studies^{13,14,15,16}. Broadly, this trend is due to the multiple components that make up the Milky Way. The disk components consist of younger metal-rich stars that reside in the plane of the Galaxy and have more circular orbits, while the halo component consists of older metal-poor stars that reside out of the plane and have more elliptical orbits.



Above we examine a more detailed relationship between chemistry and kinematics, where we plot the radius of a circular orbit with the same angular momentum as a star, x_{mix} (this acts as a de-projection of a star's velocity in the direction the Galactic rotation)¹⁷ vs. the velocity in the direction of the Galactic anti-center, U , for stars with different metallicities estimated from our relationship. In each of these figures, we see clumps in velocity space, whose substructure/morphology is found to be dependent on metallicity. For example, some of these clumps only become apparent at higher metallicities (i.e. the "Hercules Streams"¹⁸, indicated by the red ellipse), while others seem to completely change their shape as the metallicity increases (i.e. "Coma Berenices", indicated by the blue ellipse). Similar changes have been observed in past studies that utilize metallicities derived from spectroscopy¹⁹, but with our photometric metallicity relationship we have the potential to examine these changes in greater detail due to the much larger sample size available from using low-mass stars. Such a detailed study would be helpful in the understanding of the origins and histories of these streams, and how they tie into the dynamical history of the Milky Way. For example, multiple metallicity components within a stream could indicate multiple major star formation events during the stream's history. We look forward to examining such details with our newly calibrated relationship using the data from the Gaia survey.

References

1. Chambers, K. C., Magnier, E. A., Metcalfe, N., et al. 2016, arXiv e-prints, arXiv:1612.05560
2. Skrutskie, M. F., Cutri, R. M., Stiening, R., et al. 2006, AJ, 131, 1163
3. Wright, E. L., Eisenhardt, P. R. M., Mainzer, A. K., et al. 2010, AJ, 140, 1868
4. Gaia Collaboration, Brown, A. G. A., Vallenari, A., et al. 2016, A&A, 616, A1
5. Holtzman, J. A., Hasselquist, S., Shetrone, M., et al. 2018, The Astronomical Journal, 156, 125
6. Hejazi, N., Lépine, S., Homeier, D., Rich, R. M., & Shara, M. M. 2020, AJ, 159, 30
7. Buitinck, L., Louppe, G., Blondel, M., et al. 2013, in ECML PKDD Workshop: Languages for Data Mining and Machine Learning, 108–12
8. Green, G. M., Schlafly, E., Zucker, C., Speagle, J. S. & Finkbeiner, D. 2019, ApJ 887, 93
9. Schlafly, E. F. & Finkbeiner, D. P. 2011, ApJ 737, 103
10. Davenport, J. R. et al. 2014, MNRAS 440, 3430–3438
11. Schmidt, S. J., Wagoner, E. L., Johnson, J. A., et al. 2016, MNRAS, Volume 460, Issue 3, p.2611-2624, 460, 2611
12. Davenport, J. R., & Dorn-Wallenstein, T. Z. 2019, Research Notes of the American Astronomical Society, 3, 54
13. Nordström, B., Mayor, M., Andersen, J., et al. 2004, A&A, 418, 989
14. Ivezić, Ž., Sesar, B., Juríć, C. M., et al. 2008, ApJ, 684, 287
15. Bensby, T., Feltzing, S., & Oey, M. 2014, A&A, 562, A71
16. Grieves, N., Ge, J., Thomas, N., et al. 2018, MNRAS, 481, 3244
17. Hunt, J. A., Johnston, K. V., Pettitt, A. R., et al. 2020, MNRAS, arXiv:2006.03600
18. Famaey, B. et al. 2005, A&A 430, 165–186
19. Quillen, A. C. et al. 2018 MNRAS, 480, 3132–3139